

Nanoscale

Accepted Manuscript



This is an *Accepted Manuscript*, which has been through the Royal Society of Chemistry peer review process and has been accepted for publication.

Accepted Manuscripts are published online shortly after acceptance, before technical editing, formatting and proof reading. Using this free service, authors can make their results available to the community, in citable form, before we publish the edited article. We will replace this *Accepted Manuscript* with the edited and formatted *Advance Article* as soon as it is available.

You can find more information about *Accepted Manuscripts* in the [Information for Authors](#).

Please note that technical editing may introduce minor changes to the text and/or graphics, which may alter content. The journal's standard [Terms & Conditions](#) and the [Ethical guidelines](#) still apply. In no event shall the Royal Society of Chemistry be held responsible for any errors or omissions in this *Accepted Manuscript* or any consequences arising from the use of any information it contains.

Cite this: DOI: 10.1039/c0xx00000x

www.rsc.org/xxxxxx

ARTICLE TYPE

Design of highly sensitive and selective Au@NiO yolk-shell nanoreactors for gas sensor applications

Prabhakar Rai, Ji-Wook Yoon, Hyun-Mook Jeong, Su-Jin Hwang, Chang-Hoon Kwak, and Jong-Heun Lee*

5 Received (in XXX, XXX) Xth XXXXXXXXXX 20XX, Accepted Xth XXXXXXXXXX 20XX

DOI: 10.1039/b000000x

Au@NiO yolk-shell nanoparticles (NPs) were synthesized by simple solution route and applied for efficient gas sensor towards H₂S gas. Carbon capsulated Au (Au@C core-shell) NPs were synthesized by glucose-assisted hydrothermal method, whereas Au@NiO yolk-shell NPs were synthesized by precipitation method using Au@C core-shell NPs as a template. Sub-micrometer Au@NiO yolk-shell NPs were formed having 50-70 nm Au NPs at the periphery of NiO shell (10-20 nm), which was composed of 6-12 nm primary NiO particles. Au@NiO yolk-shell NPs showed higher response for H₂S compared to other interfering gases (ethanol, *p*-xylene, NH₃, CO and H₂). The maximum response was 108.92 for 5 ppm of H₂S gas at 300°C, which was approximately 19 times higher than those for the interfering gases. The response of Au@NiO yolk-shell NPs to H₂S was approximately 4 times higher than that of bare NiO hollow nanospheres. Improved performance of Au@NiO yolk-shell NPs was attributed to hollow spaces that allowed the accessibility of Au NPs to gas molecules. It was suggested that adsorption of H₂S on Au NPs resulted in formation of sulfide layer, which possibly lowered its work function, and therefore tuned the electron transfer from Au to NiO rather NiO to Au, which led to increase in resistance and therefore response.

Introduction

The concerns related to the toxic effects of chemicals on human being and its surrounding environment lead into the rapid development of gas sensors for personal safety, environmental sustainability, and so forth.¹⁻⁵ Among various toxic gases, hydrogen sulfide (H₂S) is a colorless gas with the distinct smell of rotten eggs. H₂S is extremely dangerous due to its flammability as well as its high lipid solubility, which allows it to pass through the cellular membranes in the body, forms a complex bond with iron in the mitochondrial cytochrome enzymes, thus preventing cellular respiration.⁶ It is readily produced as a byproduct from petroleum refining, farming and waste management to natural gas production.^{6,7} The odor threshold of H₂S was set to 10 ppm and at concentrations exceeding 150 ppm, H₂S is extremely toxic and hazardous.⁶⁻⁸ The human body also produces small amounts of H₂S in exhaled breath, which is used as a signaling molecule for metabolic disorder called as halitosis.⁹ These factors indicate the importance of development of low cost and more efficient sensing devices capable of detecting H₂S at low concentrations.

Metal oxide semiconductor (MOS) gas sensors, such as SnO₂, ZnO, In₂O₃, WO₃, NiO, Co₃O₄, play an important role in the detection of toxic pollutants and flammable gases.¹⁰⁻¹⁵ Nickel oxide (NiO) is a chemically and thermally stable p-type semiconductor with band gap energy equal to 3.6–4.0 eV.¹⁶ The amount of oxygen adsorption in NiO is known to be significantly

higher than other metal oxides,¹⁷ which makes it suitable candidate for gas sensing and chemical catalyst.^{16, 18-21} The malodor gases generally have relatively higher reactivity compared with the conventional VOCs, and thus easier to be detected by using metal oxide gas sensor.^{22, 23} Although, the gas sensing property of NiO is tremendously investigated, its gas-sensing performance towards H₂S is still needs to be improved. It has been reported by several researchers that the performance of gas sensors towards H₂S can be enhanced by incorporation of noble metals, such as gold.²³⁻²⁸ However, noble metals NPs are unstable against sintering due to increased mobility of the metal NPs on the support at higher temperatures, which results in a loss of catalytic activity, which is a serious problem in many applications.²⁹ In recent years, much scientific effort has been directed toward the design and fabrication of nanomaterials with controlled morphologies and tailored properties, such as metal core-semiconductor shell clusters.³⁰⁻³² In such a core-shell structure, the intrinsic optical and crystal structural characteristics of core-shell structured NPs can be maintained at high temperatures because coalescence of the core material and crystal growth of the shell materials are greatly restricted.³² Yet, efforts to utilize these core-shell structures as sensing materials in gas sensors is limited due to low accessibility of metal NPs to gas molecules, which is crucial for application in gas sensing. Recently, a hybrid of core-shell structure, with the unique properties of movable cores, hollow spaces, and the functionality of shells, has attracted tremendous interest in gas sensing,

catalysis, drug delivery and battery applications.³³⁻³⁶

Herein, for the first time, we have fabricated Au@NiO yolk-shell nanoreactors for gas sensor application. Au@C core-shell NPs are used as template for deposition of polycrystalline NiO NPs using precipitation method followed by calcination. The Au@NiO yolk-shell sensor exhibited significantly enhanced sensing performance in terms of high sensitivity and selectivity to H₂S in comparison with the hollow NiO one. It has been demonstrated that high accessibility of Au NPs to gas molecules in Au@NiO yolk-shell nanoreactors enhanced its sensing performance towards H₂S. It has been suggested that chemisorbed H₂S formed a sulfide layer on Au NPs, which possibly lowered the work function of Au NPs. The electrons are donated from the gold to the NiO, which resulted in an increase in electrical resistance of NiO, and thereby response. Therefore, Au@NiO yolk-shell nanoreactors have great potential as a high-performance sensing material for gas sensors. Furthermore, this new finding and mechanism study of Au@NiO yolk-shell nanoreactors present important results for the design of novel sensing material using other heterostructures nanomaterials.

Experimental

Materials D-Glucose, HAuCl₄, urea, ethanol, Ni(NO₃)₂·6H₂O all purchased from Sigma-Aldrich, are analytical grade and were used without further purification.

Synthesis of Carbon nanospheres The carbon nanospheres were synthesized using the method reported elsewhere with substantial modification.³⁷ In a typical procedure, 0.5 M, D-Glucose solution (50 mL) was prepared in deionized water. This solution was placed in a 100 mL Teflon lined autoclave and maintained at 180°C for 8 h. The brown-black products were separated by centrifugation, cleaned by three cycles of centrifugation/washing/redispersion in water and in ethanol, and oven-dried at 80°C for longer than 6 h.

Synthesis of Au@Carbon core-shell NPs A 2 mL, 0.01 M solution of HAuCl₄ was added to a glucose solution (50 mL, 0.5M) with stirring to form clear solutions. The subsequent procedures were the same as described above for the synthesis of carbon nanospheres.

Synthesis of Au@NiO yolk-shell NPs The Au@NiO yolk-shell NPs were synthesized by chemical precipitation of nickel nitrate followed by calcination as reported elsewhere with substantial modifications.³⁸ In a typical synthesis, Au@C NPs (100 mg) were added in 20 mL ethanol and well dispersed with the assistance of sonication for 15 min. The nickel salt and urea were readily mixed in 5 mL water and added to Au@C solution. The concentration of nickel salt and urea was fixed at 0.04 and 0.4 M, respectively. Finally, glass bottle was sealed and kept at 80°C for 24 h with vigorous stirring before the product was collected by centrifugation. The products were washed with ethanol and distilled water several and dried at 70°C for 5 h. The final metal oxide products were obtained after calcination at 450°C in static air for 3 h with a heating rate of 1 °C min⁻¹.

Characterization The crystallinity and phase of as prepared specimens were analyzed by X-ray diffraction (XRD, D/MAX-2500V/PC, Rigaku, Japan), while the morphologies were investigated by high resolution transmission electron microscopy (HR-TEM, JEM-2100F, JEOL Co. Ltd., USA). Cross section

images were taken by field-emission scanning electron microscopy (FE-SEM, S-4700, Hitachi, Japan)

Sensing device fabrication and measurement An alumina substrate (area = 1.5×1.5 mm²; thickness = 0.25 mm) with two Au electrodes on its top surface (electrode widths = 1 mm; separation = 0.2 mm) and a microheater on its bottom surface was used. Bare and Au@NiO yolk-shell NPs were dispersed in deionized water and the slurry was coated on the Au electrodes by drop-coating using a micropipette. The sensing temperatures were measured using an IR temperature sensor (Metis MP25, Sensortherm GmbH, Germany) and were controlled by the microheater underneath the alumina substrate. Heater powers of 302, 376 and 445 mW were used to heat the alumina substrates to 300, 350 and 400 °C, respectively. The sensors were contained in a specially designed, low-volume (1.5 cm³), quartz tube to minimize delays in changing their surrounding atmosphere. The sensor element was heated at 450°C for 12 h to prepare thermally stable sensors at the gas sensing temperature (300-400°C) and to remove the remaining solvents. The microstructure of the sensing layer was similar in both devices and also the thickness was below 10 μm in both devices (See Fig. S1 in supporting informants). The gas responses ($S = R_g/R_a$; R_a , resistance in air and R_g , resistance in gas) to 5 ppm of ammonia (NH₃), hydrogen sulphide (H₂S), carbon monoxide (CO), ethanol (C₂H₅OH), hydrogen (H₂), and p-xylene (1,4-dimethylbenzene, C₆H₄(CH₃)₂) were measured at 300–400°C. The gas concentrations were controlled by changing the mixing ratio of the parent gases (5 ppm ammonia, 5 ppm hydrogen sulphide, 5 ppm p-xylene, 100 ppm carbon monoxide, 100 ppm ethanol, and 100 ppm hydrogen; all in dry air balance) and dry synthetic air. The DC two-probe resistances were measured using an electrometer interfaced with a computer.

Results and Discussion

Fig. 1 shows the XRD pattern of carbon and Au@C core-shell along with their TEM images. The Au characteristic peaks are recorded at 38.07, and 44.2 belongs to (111) and (200) plane of face-centered cubic structure of Au NPs (JCPDS Card No. 04-0784). There is no peaks related to carbon is recorded either in Au@C or carbon NPs due to its amorphous nature. Furthermore, no other impurity peaks, such as Au₂O, Au₂O₃, AuCl, Au₂Cl₆ etc., are found in XRD profile, which indicates the complete reduction

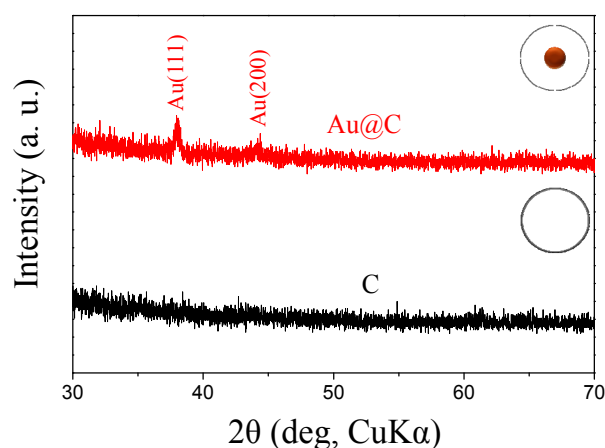


Fig. 1 XRD patterns of the pure carbon and Au@C core-shell NPs.

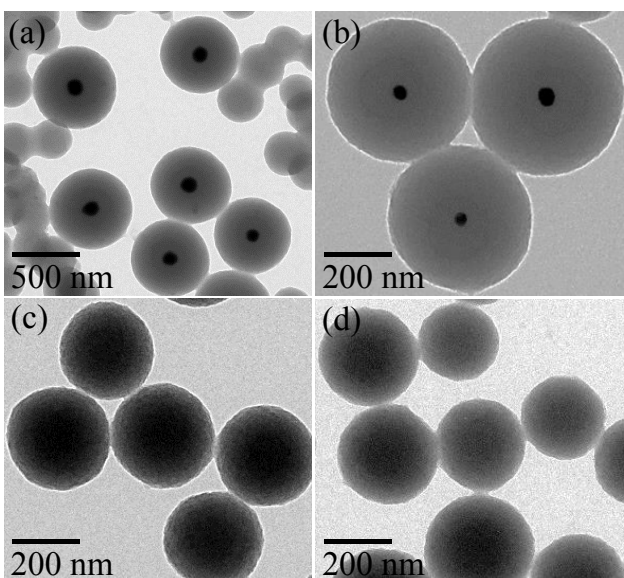


Fig. 2 TEM images of the (a, b) Au@C core-shell and (c, d) pure carbon NPs.

of Au salt into Au NPs. TEM analysis of as prepared carbon and Au@C core-shell NPs is carried out and shown in Fig. 2. TEM images clearly shows the formation of submicrometer (400-500 nm) Au@C core shell NPs, which is composed of 50-70 nm Au NPs and 200 nm carbon shells (Figs. 2a and b). TEM images also shows the presence of few free carbon nanosphers. However, in the absence of Au NPs as a core, 200-250 nm carbon spheres are formed (Figs. 2c and d).

Fig. 3 presents the XRD patterns of the hollow NiO and Au@NiO yolk-shell NPs. XRD results reveal the crystal structure of the bunsenite NiO in both specimens (JCPDS No. 47-1049). Two distinct peaks for Au NPs with (111) and (200) face-centered cubic structure are recorded in Au@NiO yolk-shell NPs (JCPDS Card No. 04-0784). No impurity phases were observed from the XRD pattern, which confirms the high purity of the product.

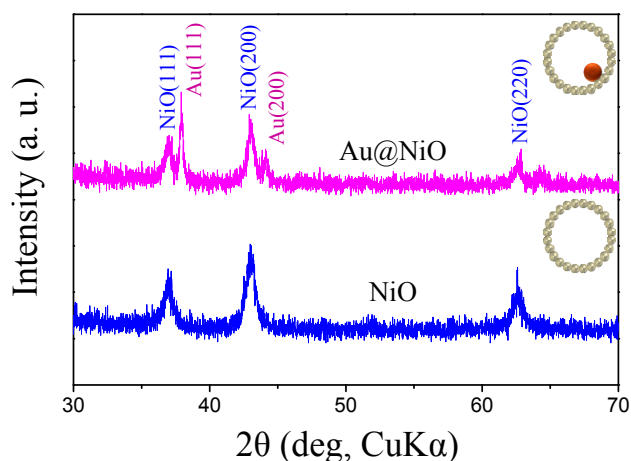


Fig. 3 XRD patterns of the hollow NiO and Au@NiO yolk-shell NPs.

Fig. 4 shows the detailed TEM analysis of hollow NiO and Au@NiO yolk-shell NPs. The formation of submicrometer yolk-shell nanostructure can be clearly seen in Fig. 4a and b. There are

few free NiO microspheres are also present, which is possibly related to presence of free carbon spheres in Au@C sample. These images clearly indicate the presence of the hollow structure with a shell wall thickness of ca. 10–20 nm. It appears that the shell is formed of closely packed 6-12 nm NiO NPs (Fig. 4c and d). The Au NPs (50-80 nm) are present at the periphery of the shell. The size of Au NPs in Au@NiO yolk-shell is almost similar to the size in Au@C core-shell NPs, which suggests that the formation of NiO shell restricts the grain growth of Au NPs during calcination. As compared to Au@C core-shell NPs, where Au NPs are present in the center, the presence of Au NPs at the periphery of the shell in Au@NiO yolk-shell confirms the formation of hollow structure. This indicates that calcination process results in the removal of carbon shell, and therefore Au NPs become free and deposited at the periphery of the NiO shell. Moreover, the interface between Au NPs and NiO shell suggests the deposition of Au NPs on NiO shell through one side leaving other part exposed (Fig. 4d). It makes yolk-shell structure significantly different than core-shell structures, where shell materials are deposited on the entire surfaces of Au NPs.³⁰⁻³² Thus, the gas accessibility of Au NPs in yolk-shell structure is better than the core-shell structures. Furthermore, selected area electron diffraction (SAED) pattern clearly indicates the presence of Au core and polycrystalline NiO shell (Fig. 4e). In the absence of Au NPs, hollow NiO nanospheres in the range of 200 nm are formed as shown in Fig. 4f. The shell wall thickness of NiO nanospheres was 20-30 nm and it is also composed of 15-20 nm primary NiO NPs.

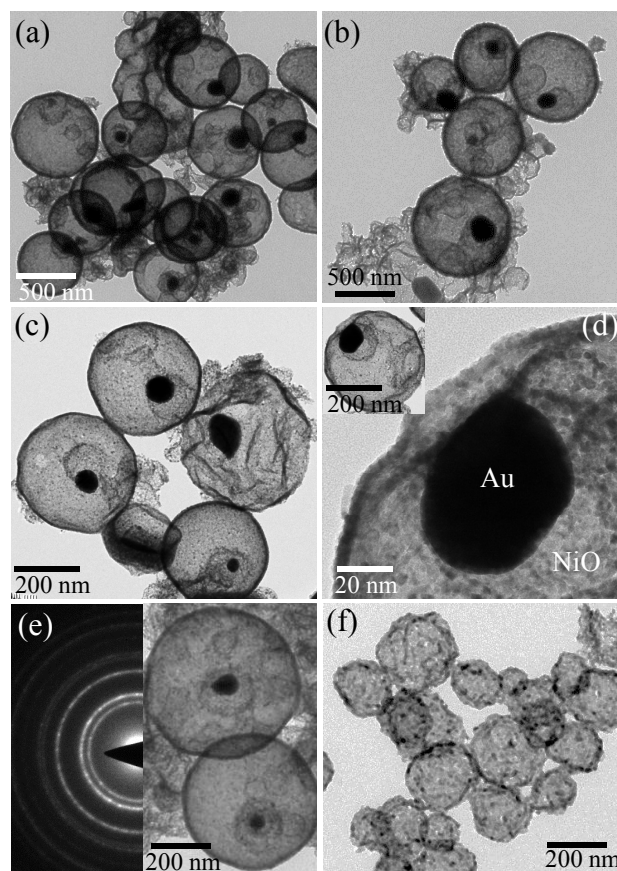


Fig. 4 TEM images of Au@NiO yolk-shell (a-e) and bare NiO NPs (f).

The formation mechanism of carbon spheres and Au@C core-shell NPs was explained by Sun et al.³⁷ They have proposed that oligosaccharides are formed in initial stage due to the polymerization of glucose. This is followed by carbonization step, where dehydration of oligosaccharides takes place. The nuclei then grew uniformly and isotropically resulted in the formation of carbon nanospheres. In Au@C core-shell NPs, first Au⁺ cations are reduced by glucose to Au NPs (Au⁰) as glucose is a strong reducing agent. This is followed by polymerization and carbonization of glucose, which resulted in the formation of Au@C core-shell NPs. However, the size of Au@C core-shell NPs is almost double the size of carbon spheres, which is possibly related to the growth of carbon shell on Au NPs (nuclei). Since, the number of Au NPs nuclei is comparatively lesser than the carbon nuclei in case of pure carbon spheres, and hence larger Au@C core-shell NPs are formed. In the NiO coating process, the alkaline condition generated due to urea decomposition leads to the precipitation of the metal cations on the surface of the carbon templates to form a nickel hydroxide (Ni(OH)₂) layer. It is known that urea decomposes slowly at a mild temperature (60°C) into CO₂ and OH⁻, coupled with a large number of -OH bonds on the surfaces of the carbon spheres. The calcination of as prepared specimen at 450°C in presence of air results in the formation of highly crystalline NiO shell and the carbon spheres were removed. Therefore, Au@NiO yolk-shell structure is formed. A schematic presentation is shown in Fig. 5 to explain the formation mechanism of Au@NiO yolk-shell nanostructures.

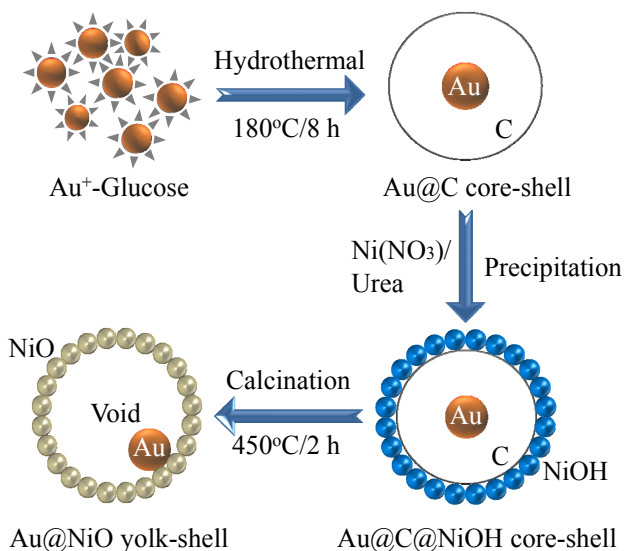


Fig. 5 Schematic presentation of the formation mechanism of Au@NiO yolk-shell NPs.

The potential applications of Au@NiO yolk-shell NPs in gas sensor was investigated for H₂S detection and displayed in Fig 6. The response characteristics of Au@NiO yolk-shell NPs towards H₂S at 400°C is displayed in Fig. 6a. It can be seen that the corresponding responses increases with the increase of H₂S concentration from 1.25 to 5 ppm. The maximum response is 44.16 recorded for 5 ppm of H₂S gas. Fig. 5b shows the response of Au@NiO yolk-shell NPs to 1.25-5 ppm of H₂S at operating temperatures from 300 to 400°C. It can be seen that response increases with decreasing testing temperature and maximum

response (108.92) recorded at 300°C for 5 ppm of H₂S gas. The response is increased approximately 2.5 times with decreasing temperature from 400°C to 300°C. However, response and recovery time increases with decrease in temperature as displayed in Fig. S2. Although, response increases with further decrease in temperature, however it was impossible to measure the response below 300°C due to fluctuation in resistance. As shown in Fig. S2, a little fluctuation in resistance at 300°C occurred, which is possibly related to very big change in resistance. Furthermore, stability and reproducibility was checked by repeating the measurement for 5 ppm of H₂S gas at 400°C for 5 days (Fig. S3). The results shows that the sensor is relatively stable

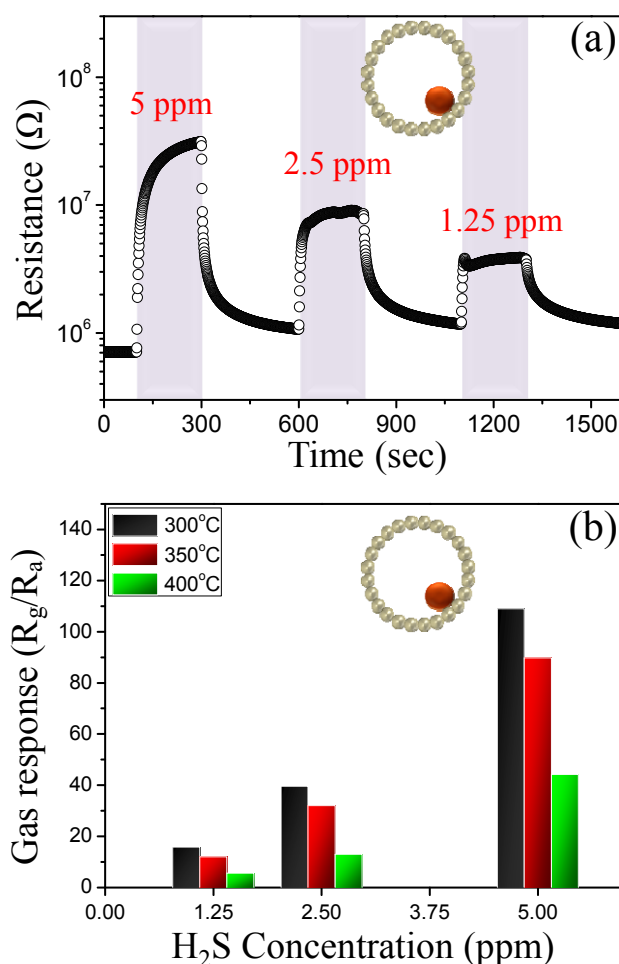


Fig. 6 (a) Response transient at 400°C and (b) Response at various temperatures for Au@NiO yolk-shell NPs.

The selectivity of Au@NiO yolk-shell NPs towards H₂S gas was measured by comparing the response for common interfering gases and displayed in Fig. 7. It can be seen that the response for H₂S is comparatively higher than other gases. Furthermore, response for H₂S increases with decreasing the temperature, whereas it has no significant effect on other gases. The response for H₂S is 7 times higher than interfering gases (maximum of xylene) at 400°C, which is increased to 19 times at 300°C (maximum of ammonia). Even for 1.25 ppm of H₂S the response was 15.75, which was higher than the 5 ppm of interfering gases

at every temperature. These results indicate the selectivity of Au@NiO yolk-shell NPs towards H₂S possibly originated due to catalytic effect of Au NPs.

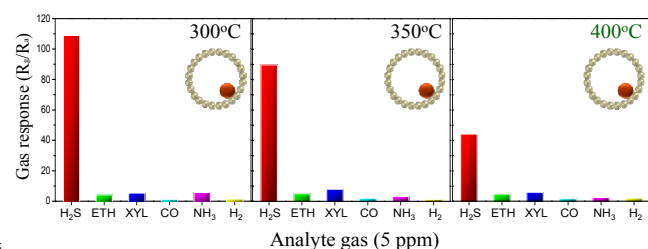


Fig. 7 Response of Au@NiO yolk-shell NPs at various temperatures (ETH for Ethanol; XYL for xylene).

Therefore, the role of Au NPs in enhancement of H₂S was investigated by comparing the H₂S sensing property of Au@NiO yolk-shell with NiO hollow spheres. The response characteristics of these two sensors towards H₂S at 400°C are displayed in Fig. 8a. The corresponding responses increased approximately 4 times for Au@NiO yolk-shell NPs (44.16) than that of pure NiO NPs (10.47). It can be seen that pure NiO sample shows a relatively low response for all gases and there is no big difference in response for H₂S with other interfering gases (Fig. 8b). However, response dramatically increased for H₂S in Au@NiO yolk-shell NPs compared to other gases, which in turn directly verifies the promotion effect of Au NPs.

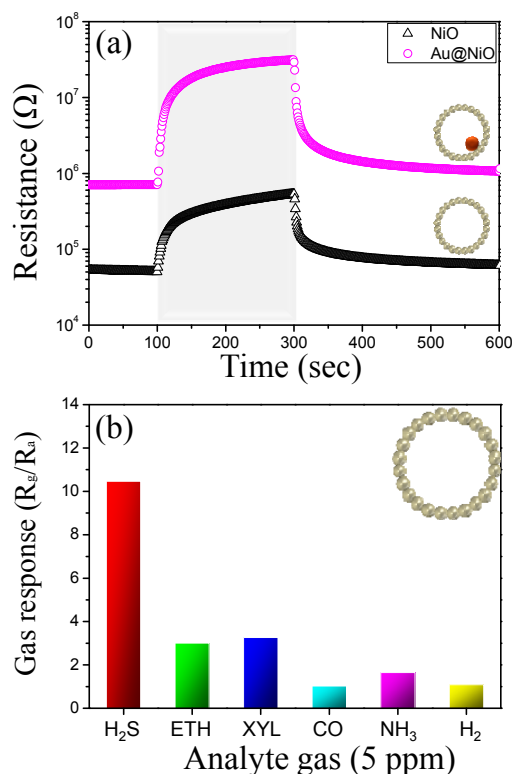
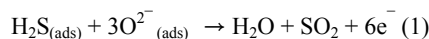


Fig. 8 (a) Response transient of Au@NiO yolk-shell NPs and NiO NPs at 400°C and (b) Response of NiO NPs at 400°C for various gases (ETH for Ethanol; XYL for xylene).

The operating principle of NiO gas sensors is based on the change of sensor conductivity by controlling mobile charge

carriers. In air atmosphere, oxygen molecules oxidized and adsorb on the surface of the NiO in the form of O₂⁻ (below 100°C), O⁻ (100-300°C), and O²⁻ ions (above 300°C) by capturing the conduction band electrons.³⁹ This transfer of electrons to oxygen species generates holes, and therefore the resistance decreases. In the environment of reducing gases, the chemisorbed oxygen anions at the surface of NiO react with these gases. The gas removes chemisorbed oxygen anions and is oxidized. Since, our sensor is operated in between 300-400°C, therefore oxygen adsorbed in the form of the O²⁻ ions, which in turn reacts with H₂S according to equation 1.



The electrons from the redox reactions between H₂S and adsorbed surface oxygen are injected into the conduction band of NiO, and the recombination between the electrons and holes results in a lower carrier concentration. Subsequently, the resistance of NiO increases, and therefore response is measured.

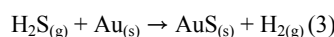
The higher sensitivity of Au@NiO yolk-shell NPs toward H₂S compare to other gases suggests the catalytic activity of Au NPs. The catalytic activity of Au NPs towards H₂S sensing has been reported by several researchers.²⁴⁻²⁸ Mubeen et al. reported H₂S sensing property of Au NPs decorated single-walled carbon nanotubes and the sensing mechanism is explained by changing the extent of electron exchange between the gold and the defect sites of SWNT when exposed to H₂S.^{26, 27} These results indicate that Au NPs functionalized on SWNT surface act as Schottky barriers and play a dominant part in hole mobility modulation by gaseous molecule interaction. In our previous study, the formation of Schottky barriers in p-type metal oxide also resulted in the decrease in baseline resistance due to transferee of conductance electrons to the Au NPs, which increased the hole mobility.³⁰ Since, the work function of NiO (5.0 eV) is slightly lower than Au NPs (5.1 eV), therefore formation of Schottky barrier in Au@NiO yolk-shell will result in decrease in resistance.^{40, 41} However, in this study, the baseline resistance of Au@NiO yolk-shell is higher than the NiO NPs (Fig. 8a). It indicates that there is no electronic interaction between Au core and NiO shell. This is possible only when Au NPs core is movable inside the NiO shell. In this situation, the interaction between Au and NiO could be due to Van der Waals forces, and therefore it is possible that there is no charge transfer or Schottky barrier modulation takes place between the Au NPs and NiO, unlike what is happening in core-shell NPs.³⁰⁻³² However, there is no clear evidence of presence of movable core in Au@NiO yolk-shell. Furthermore, the stability test of Au@NiO yolk-shell shows no drift in baseline resistance (Fig. S3 see supporting information), which indicates that the Au NPs are strongly attached to NiO shell. Since, Au@NiO yolk-shells were synthesized after calcination at 450°C for 2 h, therefore there is great possibility of a strong attachment of Au NPs to the inner wall of NiO shell. Thus, the higher baseline resistance of Au@NiO compared to NiO is possibly related to their morphology, such as shape and size. Since, the size of Au@NiO yolk-shell NPs is larger than NiO NPs, which may possibly be the reason for its high baseline resistance (Fig. 4). A relationship between numbers of grains and resistance is established by Tamaki et al., which state that resistance is directly proportional

to the number of grains between two electrodes.⁴²

$$R_a = 2R_a(i) + (N - 1) R_a(gb) = (2R_a(i) - R_a(gb)) + R_a(gb)N \quad (2)$$

Here, $R_a(i)$ and $R_a(gb)$ are resistances at interface and grain boundary in the air, respectively, and N is the number of grains included in the gap. Since, grain size in NiO nanospheres is larger than Au@NiO yolk-shell NPs, which means lesser numbers of grain boundaries are present in between two electrodes for NiO nanospheres than Au@NiO yolk-shell NPs (Fig. S4 see supporting informations). Therefore, the baseline resistance can be higher in Au@NiO yolk-shell NPs compared to NiO nanospheres.

Thus, the anomalous sensing behavior of Au@NiO yolk-shell NPs, where no significant variation in response of other gases compared to H₂S, can be explained by catalytic activity of Au NPs towards H₂S gas. There is strong possibility of adsorption of H₂S molecules on Au NPs as a result of the strong chemical affinity between Au and S ($D_{298}^0 = 418 \pm 25 \text{ kJ mol}^{-1}$).⁴³ The adsorption of H₂S has also been studied by several researchers on the clean Au(111) or (110) surface and their results shows the evidence of the adsorption of S or HS.



Accordingly, it is suggested that H₂S is chemisorbed on the Au NPs and undergoes decomposition to form either Au-SH or Au-S species on the surface of the particles. This in turn produces a sulfide shell, which lowers the surface work function of the Au NPs. It has been reported by several researchers that formation of sulfide shell of on Au NPs lower the surface work function as much as 1 eV.^{26, 44} If, there is a Schottky barrier formation between Au and NiO, such changes in the electronic state of Au NPs can tune the extent of electron exchange between the Au NPs and NiO. As the work function of the Au NPs is reduced, electrons are donated from the Au NPs to the NiO, which results in an increase in electrical resistance of NiO. Therefore, the response Au@NiO yolk-shell NPs increases for H₂S compared to other gases, as similar phenomenon can not occur in other interference gases. A schematic presentation of possible sensing mechanism is given in Fig. 9.

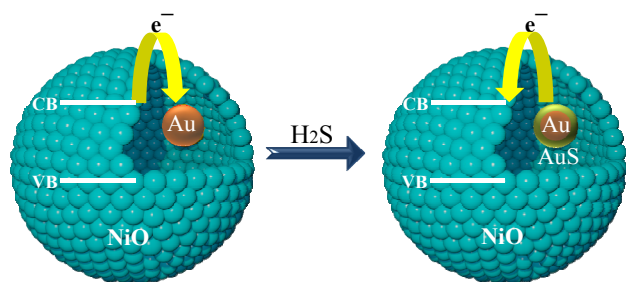
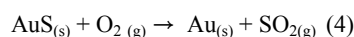


Fig. 9 Schematic diagram of H₂S sensing mechanism in Au@NiO yolk-shell NPs.

In presence of air, AuS further oxidized to produce Au NPs and SO₂.



In another hypothesis, Yoo et al suggested that the donation of electrons to the protons released in the reaction (Eq. 2) is also responsible for the change in resistance of the sensing materials.⁴⁵

Thus, the increase in response of Au@NiO yolk-shell NPs toward H₂S compare to other gases is possibly related to doping effect caused by the release of protons after the reaction between the Au NPs and H₂S.

The increase in response with decrease in temperature is related to catalytic effect of Au NPs, as its catalytic activity increases towards H₂S at low temperature. It is also supported from sensing result of other common interfering gases, which shows no significant variation in response with temperature. Furthermore, the resistance of the Au@NiO yolk-shell NPs increased with a decrease in temperature, indicating that the current conduction path is through the semiconducting NiO, as the resistance decreases with a decrease in temperature for metals. This increase in resistance is related to decrease in carrier concentration with decreasing temperature. Furthermore, the baseline resistance depends on the height of the potential energy barrier to carrier transport between neighboring grains in the metal oxide, which is a function of temperature. If we consider a migration transport path with resistance R_m , then R_m increases exponentially according to equation (5).

$$R_m = R_{m0} \exp\left(\frac{eV_s}{RT}\right) \quad (5)$$

where, V_s is the double potential energy barrier height, RT is the thermal energy, and R_{m0} is the resistance at $V_s = 0$. Thus, the resistance decreases with increasing temperature.

Furthermore, the increase in recovery time with decreasing temperature is possibly related to SO₂ poisoning i. e. the adsorption of SO₂ gas on the surface sites of NiO, which decrease the active sites for oxygen adsorption. Thus, it makes difficult to recover the sensor resistance at low temperature, however with increasing temperature recovery time decreases due to the promotion of SO₂ desorption

Conclusions

Yolk-shell Au@NiO NPs were synthesized by chemical precipitation method. Au@C core-shell NPs were synthesized by glucose-assisted hydrothermal method, where 50-70 nm Au NPs were covered with 200 nm carbon shell. Au@NiO yolk-shell NPs were synthesized by chemical precipitation and calcination of nickel salt using Au@C core-shell NPs as a template. Sub-micrometer Au@NiO NPs yolk-shell NPs were formed having 50-80 nm Au NPs at the periphery of NiO shell. The maximum response of Au@NiO NPs yolk-shell NPs was 108.92 at 300°C for 5 ppm of H₂S gas. The response of Au@NiO yolk-shell NPs was decreased with increasing testing temperatures and decreasing gas concentrations. The H₂S response of Au@NiO NPs yolk-shell NPs was 19 times higher than the interfering gases at 300°C. Even for 1.25 ppm of H₂S the response was 15.75, which was higher than the 5 ppm of interfering gases at every temperature. The H₂S response of Au@NiO yolk-shell NPs was approximately 4 times higher than that of bare NiO NPs. It was suggested that adsorption of H₂S on Au NPs changed its electronic state, where Au NPs donated the electron to NiO NPs, which in turn increases the resistance and thereby response. Thus, hollow spaces allowed the accessibility of Au NPs to gas molecules, which in turn improved the gas sensing performance of Au@NiO yolk-shell NPs.

Acknowledgment

This work was supported by the National Research Foundation of Korea (NRF) (No. 2013R1A2A1A01006545).

Notes and references

^s *Department of Materials Science and Engineering, Korea University, Seoul 136-713, Republic of Korea. E-mail: jongheum@korea.ac.kr; Fax: +82-2-928-3584; Tel: +82-2-3290-3282*

† Electronic Supplementary Information (ESI) available: [Cross section SEM image of Au@NiO and NiO NPs sensing layer, Response transient of Au@NiO yolk-shell NPs at various temperatures and concentrations of H₂S, stability test of Au@NiO yolk-shell NPs at 400°C for 5 ppm of H₂S for 5 days and schematic diagram of conduction of current in NiO and Au@NiO yolk-shell NPs containing grain boundaries]. See DOI: 10.1039/b000000x/

- 1 J. Kong, N. R. Franklin, C. W. Zhou, M. G. Chapline, S. Peng, K. J. Cho and H. J. Dai, *Science*, 2000, **287**, 622–625.
- 2 A. Kolmakov and M. Moskovits, *Annu. Rev. Mater. Res.*, 2004, **34**, 151–180.
- 3 D. H. Zhang, Z. Q. Liu, C. Li, T. Tang, X. L. Liu, S. Han, B. Lei and C. W. Zhou, *Nano Lett.*, 2004, **4**, 1919–1924.
- 4 Q. F. Pengfei, O. Vermesh, M. Grecu, A. Javey, O. Wang, H. J. Dai, S. Peng and K. J. Cho, *Nano Lett.*, 2003, **3**, 347–351.
- 5 J. Li, Y. J. Lu, Q. Ye, M. Cinke, J. Han and M. Meyyappan, *Nano Lett.*, 2003, **3**, 929–933.
- 6 R. J. Reiffenstein, W. C. Hulbert and S. H. Roth, *Annu. Rev. Pharmacol. Toxicol.*, 1992, **32**, 109–134.
- 7 R. G. Hendrickson, A. Chang and R. J. Hamilton, *Am. J. Ind. Med.*, 2004, **45**, 346–350.
- 8 R. O. Beauchamp, J. S. Bus, J. A. Popp, C. J. Boreiko, D. A. Andjelkovich and P. Leber, *Crit. Rev. Toxicol.*, 1984, **13**, 25–97.
- 9 K.-I. Choi, H.-J. Kim, Y. C. Kang and J.-H. Lee, *Sens. Actuators B*, 2014, **194**, 371–376.
- 10 H.-R. Kim, K.-I. Choi, K.-M. Kim, I.-D. Kim, G. Cao and J.-H. Lee, *Chem. Commun.*, 2010, **46**, 5061–5063.
- 11 P. Rai, W.-K. Kwak and Y.-T. Yu, *ACS Appl. Mater. Interfaces*, 2013, **5**, 3026–3032.
- 12 X. Zou, J. Wang, X. Liu, C. Wang, Y. Jiang, Y. Wang, X. Xiao, J. C. Ho, J. Li, C. Jiang, Y. Fang, W. Liu and L. Liao, *Nano Lett.*, 2013, **13**, 3287–3292.
- 13 H. G. Moon, Y.-S. Shim, D. H. Kim, H. Y. Jeong, M. Jeong, J. Y. Jung, S. M. Han, J. K. Kim, J.-S. Kim, H.-H. Park, J.-H. Lee, H. L. Tuller, S.-J. Yoon and H. W. Jang, *Sci Rep.*, 2012, **2**, 588.
- 14 H.-J. Kim, J.-W. Yoon, K.-I. Choi, H. W. Jang, A. Umar and J.-H. Lee, *Nanoscale*, 2013, **5**, 7066–7073.
- 15 H. Nguyen and S. A. El-Safty, *J. Phys. Chem. C*, 2011, **115**, 8466–8474.
- 16 H. Steinebach, S. Kannan, L. Rieth and F. Solzbacher, *Sens. Actuators B*, 2010, **151**, 162–168.
- 17 M. Iwamoto, Y. Yoda, N. Yamazoe and T. Seiyama, *J. Phys. Chem.*, 1978, **82**, 2564–2570.
- 18 N. G. Cho, H.-S. Woo, J.-H. Lee and I.-D. Kim, *Chem. Commun.*, 2011, **47**, 11300–11302.
- 19 C. Luyoa, R. Ionescu, L.F. Reyesa, Z. Topalian, W. Estrada, E. Llobet, C.G. Granqvist and P. Heszlerd, *Sens. Actuators B*, 2009, **138**, 14–20.
- 20 N. G. Cho, I.-S. Hwang, H.-G. Kim, J.-H. Lee, I.-D. Kim, *Sens. Actuators B*, 2011, **155**, 366–371.
- 21 G. Bai, H. Dai, J. Deng, Y. Liu and K. Ji, *Catal. Commun.*, 2012, **27**, 148–153.
- 22 F. Zhang, A. Zhu, Y. Luo, Y. g Tian, J. Yang and Y. Qin, *J. Phys. Chem. C*, 2010, **114**, 19214–19219.
- 23 K.-Y. Dong, J.-K. Choi, I.-S. Hwang, J.-W. Lee, B. H. Kang, D.-J. Ham, J.-H. Lee and B.-K. Ju, *Sens. Actuators B*, 2011, **157**, 154–161.
- 24 J.-W. Yoon, Y. J. Hong, Y. C. Kang and J.-H. Lee, *RSC Advances*, 2014, DOI: 10.1039/x0xx00000x.
- 25 C. Liu, K. Hayashi and K. Toko, *Sens. Actuators B*, 2012, **161**, 504–509.
- 26 S. Mubeen, T. Zhang, N.a Chartuprayoon, Y. Rheem, A. Mulchandani, N. V. Myung and M. A. Deshusses, *Anal. Chem.*, 2010, **82**, 250–257.
- 27 S. Mubeen, J.-H. Lim, A. Srirangarajan, A. Mulchandani, M. A. Deshusses and N. V. Myung, *Electroanalysis*, 2011, **23**, 2687–2692.
- 28 M. D. Shirsat, M. A. Bangar, M. A. Deshusses, N. V. Myung, and A. Mulchandani, *Appl. Phys. Lett.*, 2009, **94**, 083502.
- 29 P. M. Arnal, M. Comotti and F. Schu^uth, *Angew. Chem. Int. Ed.*, 2006, **45**, 8224–8227.
- 30 P. Rai, R. Khan, S. Raj, S. M. Majhi, K.-K. Park, Y.-T. Yu, I.-H. Lee and P. K. Sekhar, *Nanoscale*, 2014, **6**, 581–588.
- 31 Y.-T. Yu and P. Dutta, *Sens. Actuators B*, 2011, **157**, 444–449.
- 32 Y.-S. Kim, P. Rai and Y.-T. Yu, *Sens. Actuators B*, 2013, **186**, 633–639.
- 33 L. Wang, H. Dou, Z. Lou and T. Zhang, *Nanoscale*, 2013, **5**, 2686–2691.
- 34 S. Wang, M. Zhang and W. Zhang, *ACS Catal.*, 2011, **1**, 207–211.
- 35 J. Liu, S. Z. Qiao, S. B. Hartono and G. Q. Lu, *Angew. Chem. Int. Ed.*, 2010, **49**, 4981–4985.
- 36 Z. Sun, K. Xie, Z. A. Li, I. Sinev, P. Ebbinghaus, A. Erbe, M. Farle, W. Schuhmann, M. Muhler and E. Ventosa, *Nat. Commun.*, 2013, **4**, 1331.
- 37 X. Sun and Y. Li, *Angew. Chem. Int. Ed.*, 2004, **43**, 597–601.
- 38 J. H. Pan, Q. Huang, Z. Y. Koh, D. Neo, X. Z. Wang and Q. Wang, *ACS Appl. Mater. Interfaces*, 2013, **5**, 6292–6299.
- 39 M. Takata, D. Tsubone and H. Yanagida, *J. Am. Ceram. Soc.*, 1976, **59**, 4–8.
- 40 M. D. Irwin, D. B. Buchholz, A. W. Hains, R. P. H. Chang and T. J. Marks, *PNAS*, 2008, **105**, 2783–2787.
- 41 A. Younis, D. Chu, X. Lin, J. Yi, F. Dang and S. Li, *ACS Appl. Mater. Interfaces*, 2013, **5**, 2249–2254.
- 42 J. Tamaki, Y. Nakataya and S. Konishi, *Sens. Actuators B*, 2008, **130**, 400–404.
- 43 J. Geng, M. D. R. Thomas, D. S. Shephard and B. F. G. Johnson, *Chem. Commun.*, 2005, 1895–1897.
- 44 V. De Renzi, R. Rousseau, D. Marchetto, R. Biagi, S. Scandolo and U. del Pennino, *Phys. Rev. Lett.*, 2005, **95**, 046804.
- 45 K. S. Yoo, I. W. Sorensen and W. S. Glaunsinger, *J. Vac. Sci. Technol. A*, 1994, **12**, 192–198.